Research Square

Preprints are preliminary reports that have not undergone peer review.
They should not be considered conclusive, used to inform clinical practice,
or referenced by the media as validated information.

Europium-doped hydroxyapatite nanorods suppress lipopolysaccharide-induced inflammation in human periodontal ligament cells and attenuate alveolar bone loss in experimental periodontitis

Yangyang Jiang
Shanghai Ninth People's Hospital
Junqin Lu
Shanghai East Hospital
Tiancheng Li
Shanghai Ninth People's Hospital
Cheng Zhu
Shanghai Ninth People's Hospital
Ruomei Li
Shanghai Ninth People's Hospital
Zhiyu Zhu
Shanghai Ninth People's Hospital
Jin Hao
Shanghai Ninth People's Hospital
Lunguo Xia
Shanghai Ninth People's Hospital
Bing Fang
fangbing@sjtu.edu.cn

Shanghai Ninth People's Hospital

Research Article

Keywords:

Posted Date: November 11th, 2026

DOI: https://doi.org/10.21203/rs.3.rs-11300135/v1

License: This work is licensed under a Creative Commons Attribution 4.0 International License.
Read Full License

Additional Declarations: No competing interests reported.

Europium-doped hydroxyapatite nanorods suppress lipopolysaccharide-induced inflammation in human periodontal ligament cells and attenuate alveolar bone loss in experimental periodontitis

Running title: Europium-doped hydroxyapatite in experimental periodontitis

Yangyang Jiang[a,1], Junqin Lu[b,1], Tiancheng Li[a], Cheng Zhu[a], Ruomei Li[a], Zhiyu Zhu[a], Jin Hao[a,*], Lunguo Xia[a,*], Bing Fang[a,*]

[1] Yangyang Jiang and Junqin Lu contributed equally to this work.

* Correspondence: Jin Hao, Lunguo Xia and Bing Fang

[a] Department of Orthodontics, Shanghai Ninth People's Hospital, Shanghai Jiao Tong University School of Medicine, College of Stomatology, Shanghai Jiao Tong University, National Center for Stomatology, National Clinical Research Center for Oral Diseases, Shanghai Key Laboratory of Stomatology, Shanghai Research Institute of Stomatology, Shanghai 200011, China

[b] Department of Stomatology, Shanghai East Hospital, School of Medicine, Tongji University, Shanghai 200120, China

Correspondence address: 500 Quxi Road, Shanghai 200011, China.

haojin6352@sjtu.edu.cn (Jin Hao), xialunguo@hotmail.com (Lunguo Xia), fangbing@sjtu.edu.cn (Bing Fang).

Article type: Research Article. Main text: 3881 words. Abstract: 245 words. **Figures:** 6. Main tables: 0. **References:** 24. Supplementary material: **Online** Resource 1 (Fig. S1 and Tables S1–S4).

Abstract

Objectives To compare the effects of europium-doped hydroxyapatite (Eu-HAP) and undoped hydroxyapatite (HAP) on primary human periodontal ligament cells after lipopolysaccharide (LPS) withdrawal and on alveolar bone in experimental periodontitis.

Materials and Methods PEGylated nanorods were characterized and tested at 10 μg/mL in cells from three donors after a 24-h LPS challenge and washout. We measured inflammatory and osteogenic transcripts and alkaline phosphatase activity. Ligature-treated rats received bilateral gingival injections of saline, HAP or Eu-HAP on seven dates from days 7 to 25. Micro-CT and histology were assessed on day 28 (four rats/group).

Results Eu-HAP contained 8.0 wt% Eu (12.5 mol% of total Eu and Ca, versus 5% in the feed); its hydrodynamic diameter was 321 nm by dynamic light scattering. Compared with HAP, Eu-HAP lowered *TNF* and *IL1B* expression and increased *ALPL* and *SPP1* expression; *RUNX2* did not differ. *IL1B* expression was 1.5 times the unchallenged mean with Eu-HAP and 5.3 times that mean after LPS alone. At day 28, Eu-HAP yielded a shorter cemento-enamel junction–alveolar bone crest distance than HAP (0.44 vs 0.58 mm; P = 0.0406) and a higher bone volume fraction (80% vs 73%; P = 0.0492). Osteoclast density was 21 versus 39 cells/mm².

Conclusions Eu-HAP reduced inflammatory transcripts and enhanced selected osteogenic responses after LPS withdrawal. In rats, local Eu-HAP preserved more alveolar bone at the endpoint than HAP.

Clinical Relevance The findings support preclinical evaluation of Eu-HAP for periodontal bone preservation. Its benefit alongside standard periodontal care remains unknown.

Keywords Periodontitis; Hydroxyapatite; Europium; Periodontal ligament cells; Alveolar bone loss; Nanomaterials

Introduction

Periodontitis is a dysbiosis-driven chronic inflammatory disease that destroys the periodontal ligament and alveolar bone; its severe form affects roughly one in ten adults and remains a leading cause of tooth loss [1, 2]. Subgingival instrumentation, the cornerstone of guideline-based care, controls the microbial burden but does not rebuild the attachment already lost, and regenerative procedures are reserved for selected defects and undertaken only after inflammation has been brought under control [3]. This sequencing reflects a biological constraint. Materials placed into an inflamed site must function under continuing bacterial challenge, high local cytokine concentrations and active osteoclast recruitment, conditions under which conventional osteoconductive fillers perform poorly [4].

Human periodontal ligament cells (hPDLCs), which contain fibroblastic and progenitor populations involved in ligament maintenance and periodontal repair, are directly exposed to inflammatory signals. Bacterial lipopolysaccharide (LPS) shifts hPDLCs toward a pro-inflammatory phenotype, increasing TNF-α and IL-1β output while suppressing RUNX2, alkaline phosphatase and osteopontin, and thereby their osteogenic differentiation [5–7]. Supporting these cells during recovery from inflammatory injury is therefore a relevant objective for locally delivered periodontal biomaterials.

Hydroxyapatite (HAP) is chemically similar to bone mineral and widely used as an osteoconductive filler [8]. Ionic modification can extend its biological functions. Europium-containing calcium phosphates have been investigated for bone reconstruction and osteogenic differentiation [9–12], while other europium-containing nanomaterials have shown immunomodulatory and angiogenic effects [13, 14]. Europium-containing nanospheres also suppress RANKL-induced osteoclastogenesis, with changes in reactive oxygen species and NF-κB signalling [15]. We recently reported immunomodulatory effects of Eu-HAP nanorods in osteochondral repair [11] and reduced ligature-induced alveolar bone loss with ion-doped HAP nanowires [16]. These findings motivate evaluation of Eu-HAP in periodontal disease, where resident ligament cells and alveolar bone are exposed to a distinct inflammatory environment.

Here we compared PEGylated Eu-HAP with europium-free HAP nanorods in primary hPDLCs and a rat ligature model (Fig. 1). Cells were treated after a 24-h LPS challenge and washout to evaluate recovery from an inflammatory insult. Local administration in rats began 7 days after ligature placement and continued while the ligatures remained in place. The study tests whether the Eu-HAP formulation improves inflammatory and osteogenic readouts after LPS exposure and preserves alveolar bone at the four-week endpoint, extending previous work on europium-containing apatites to periodontal disease.

Materials and methods

Study design and ethics

The study comprised physicochemical characterization of Eu-HAP and HAP nanorods, an experiment in primary hPDLCs following LPS challenge and washout, and an experiment in a rat ligature model. Animal procedures were approved by the Laboratory Animal Ethics Committee of Shanghai Ninth People's Hospital, Shanghai Jiao Tong University School of Medicine (SH9H-2023-A825-1) and are reported with reference to ARRIVE 2.0 [17]. Collection and use of periodontal ligament tissue from the donors described below were covered by approval SH9H-2024-T251-1 from the Ethics Committee of Shanghai Ninth People's Hospital. Written informed consent was obtained from donors; parental or legal-guardian consent was additionally obtained for minors.

Materials

Oleic acid, octadecylamine, europium(III) nitrate hydrate, cyclohexane, HS-PEG1000 and 2,2-dimethoxy-2-phenylacetophenone (DMPA) were purchased from Aladdin (Shanghai, China); sodium fluoride, trisodium phosphate, calcium nitrate tetrahydrate, tetrahydrofuran, chloroform and anhydrous ethanol from Beijing Chemical Works (Beijing, China). α-Minimum essential medium (α-MEM), fetal bovine serum (FBS), penicillin–streptomycin and trypsin–EDTA were from Gibco; Cell Counting Kit-8 (CCK-8) from Dojindo; calcein-AM/propidium iodide, alkaline phosphatase (ALP), Alizarin Red S and DAPI reagents from Beyotime; TRIzol from Thermo Fisher Scientific; PrimeScript RT Master Mix and TB Green Premix Ex Taq from Takara; β-glycerophosphate and L-ascorbic acid from Macklin; and Escherichia coli LPS (L2630) from Sigma-Aldrich.

Synthesis and PEGylation of Eu-HAP and HAP nanorods

Oleate-capped Eu-HAP nanorods were synthesized by a hydrothermal method adapted from Hui and Wang [18]. Octadecylamine (0.5 g) and oleic acid (4 mL) were heated with stirring until dissolved, and anhydrous ethanol (16 mL), $Ca(NO_3)_2$ (0.28 M, 6.65 mL), $Eu(NO_3)_3$ (0.28 M, 0.35 mL), NaF (0.28 M, 1.4 mL) and Na_3PO_4 (0.16 M, 7 mL) were added in sequence, giving a nominal Eu/(Ca + Eu) molar fraction of 5%. After 10 min of stirring, the mixture was sealed in a 40-mL Teflon-lined autoclave and heated at 180 °C for 12 h. The product was washed three times each with cyclohexane and ethanol and dispersed in cyclohexane. HAP nanorods were prepared by the same procedure with $Eu(NO_3)_3$ replaced by an equal volume of $Ca(NO_3)_2$ solution.

To render the nanorods water-dispersible, HS-PEG1000 was grafted onto the oleate ligands by thiol–ene photoclick chemistry [19]. Oleate-capped nanorods were dispersed in 2 mL of tetrahydrofuran, mixed with HS-PEG1000 (200 mg) and DMPA (100 µL, 10 mg/mL in tetrahydrofuran) and irradiated at 365 nm for 60 min in an ice bath with stirring. PEGylated nanorods were collected by centrifugation (12,000 rpm, 15 min), washed three times each with chloroform and ethanol, and dispersed in water. This aqueous dispersion was used for all biological experiments.

Physicochemical characterization

Morphology was examined by transmission electron microscopy (TEM; JEM-2100F, JEOL) and elemental distribution by energy-dispersive X-ray mapping (X-MAX 250, Oxford Instruments) at 200 kV. X-ray diffraction (XRD) patterns of vacuum-dried, ground samples were recorded with Cu Kα radiation (λ = 1.5406 Å) from 10° to 80° 2θ at 40 kV and 25 mA (SmartLab SE, Rigaku) and compared with the hydroxyapatite reference (JCPDS 09-0432). Fourier-transform infrared (FTIR) spectra were recorded from 4000 to 400 cm^{-1} at 4 cm^{-1} resolution (Nicolet iS20, Thermo Scientific). Bulk Ca, P and Eu content was measured by inductively coupled plasma optical emission spectrometry (ICP-OES; Agilent 5110) after microwave digestion in aqua regia. Hydrodynamic diameter, polydispersity index and zeta potential were measured at 25 °C (Zetasizer Nano ZS90, Malvern) in deionized water (0.1% w/v, pH 7) after 3 min of sonication, with three readings per sample.

Isolation and culture of primary hPDLCs

Periodontal ligament tissue was scraped from the middle third of the roots of clinically healthy premolars extracted for orthodontic reasons and cultured as explants in α-MEM containing 10% heat-inactivated FBS and 1% penicillin–streptomycin at 37 °C in 5% CO_2, with medium changed every 3 days. Outgrowing cells at passages 3–5 were used. For all in vitro experiments, each independent culture was derived from a separate donor; n = 3 donors.

LPS challenge and treatment groups

Cells were allowed to attach for 24 h and challenged with LPS (100 ng/mL) for 24 h. LPS was then washed out and the medium replaced with fresh medium containing HAP or Eu-HAP; LPS was not replenished. Four groups were compared: untreated control (Blank), LPS followed by material-free medium (LPS), LPS followed by HAP (10 μg/mL), and LPS followed by Eu-HAP (10 μg/mL). The latter two groups are labelled LPS + HAP and LPS + Eu-HAP in the figures; the plus sign denotes sequential treatment. Inflammatory readouts were collected after 4 days of treatment and osteogenic readouts on days 4, 7 and 21. Concentration screening used 0–200 μg/mL for cytocompatibility and 0–50 μg/mL for osteogenic assays. In the osteogenic screening experiments, Blank denotes cultures without LPS and 0 μg/mL denotes LPS-challenged cultures without material.

Cytocompatibility

For live/dead staining, cells seeded at 4×10^4 per well in 24-well plates were exposed for 48 h to HAP or Eu-HAP at 0–200 μg/mL, incubated with calcein-AM and propidium iodide for 30 min at 37 °C and imaged by fluorescence microscopy. For CCK-8 assays, cells seeded at 5×10^3 per well in 96-well plates were treated over the same concentration range; 10 μL of CCK-8 reagent was added to 100 μL of medium on days 1, 4 and 7, and absorbance was read at 450 nm (reference 630 nm) after 2 h.

Intracellular DCF fluorescence

After LPS challenge and 4 days of material treatment, cells were incubated with 10 μM DCFH-DA (Beyotime) for 20 min at 37 °C in serum-free medium, counterstained with Hoechst 33342 (5 μg/mL) for 10 min, washed twice with pre-warmed PBS and imaged immediately at identical acquisition settings (Leica); five to seven non-overlapping fields were recorded per well.

Osteogenic induction, ALP assays and Alizarin Red S staining

Osteogenic medium consisted of α-MEM with 10% FBS, 10 mM β-glycerophosphate, 50 μg/mL L-ascorbic acid, 100 nM dexamethasone and 1% penicillin–streptomycin. On day 4, ALP was visualized histochemically and quantified by hydrolysis of p-nitrophenyl phosphate at 405 nm, normalized to total protein determined by BCA assay. On day 21, cultures were fixed in 4% paraformaldehyde and stained with 1% Alizarin Red S (pH 4.2) [20].

RNA isolation and quantitative reverse-transcription PCR

Total RNA was extracted with TRIzol and reverse-transcribed with PrimeScript RT Master Mix. Quantitative PCR was performed with TB Green Premix Ex Taq on a QuantStudio system (95 °C for 10 min; 40 cycles of 95 °C for 15 s and 60 °C for 30 s). Relative expression was calculated by the $2^{-\Delta\Delta Ct}$ method with *GAPDH* as the reference gene. Primer sequences are listed in Online Resource Table S1 and amplification and melt curves are shown in Online Resource Fig. S1.

Immunofluorescence

Cells were fixed in 4% paraformaldehyde, blocked with bovine serum albumin and incubated overnight at 4 °C with primary antibodies against TNF-α, IL-1β, ALP, RUNX2 or osteopontin (OPN; Servicebio; Online Resource Table S2), followed by Cy3-conjugated goat anti-rabbit IgG (1:400; GB25303, Servicebio) for 50 min, FITC-phalloidin (1:200; G1041) and DAPI (G1012). Images were acquired by confocal microscopy at identical settings across groups. Immunofluorescence images from the same three independent donors are presented as

qualitative observations; fluorescence intensity and positive-cell fractions were not quantified or used for statistical inference.

Rat ligature model and local administration

Sixteen male Sprague–Dawley rats (5 weeks old, 180–220 g; Shanghai Bikai Keyi Biotechnology Co., Ltd.) were acclimatized for 1 week and allocated by body-weight-stratified block randomization to four groups (n = 4 rats/group): untreated control, ligature + saline, ligature + HAP and ligature + Eu-HAP. Group size was informed by effects observed in our previous work using this model [16]; no formal a priori power calculation was performed. Under anaesthesia (intraperitoneal Zoletil–Domitor–saline, 0.25 mL/100 g), a 0.2-mm orthodontic wire ligature was placed around maxillary first molars [21, 22]. Ligatures remained in place until the day-28 endpoint and were checked daily. On days 7, 10, 13, 16, 19, 22 and 25, each rat in the three ligature groups received one injection per side into the palatal gingiva between the first and second molars (14 injections per rat). The saline, HAP and Eu-HAP groups received the same volume (20 μL per side) by the same needle path. HAP and Eu-HAP were suspended in sterile saline at 10 μg/mL. Each HAP or Eu-HAP injection contained 0.2 μg of material. At 8.0 wt% Eu, the Eu-HAP group received 16 ng Eu per site per dosing date and 224 ng Eu per rat in total. No injection was given on day 28. The concentration was selected from the in vitro effective range; the three-day interval was empirical and informed by our previous ligature study [16]. Rats received postoperative analgesia and were monitored for predefined humane endpoints (body-weight loss above 15%, impaired feeding, abscess formation or self-injury); none reached an endpoint or was excluded. Rats were euthanized by isoflurane overdose on day 28. Specimens were coded, and micro-CT and histological measurements were performed by an investigator blinded to group allocation.

Micro-computed tomography

Maxillae were fixed in 4% paraformaldehyde for 48 h and scanned (SkyScan 1176, Bruker; 85 kV, 200 μA, 9.065255 μm pixel size, 240 ms exposure, analysis threshold 90–255). Images were reconstructed in NRecon and rendered in CTVox. The cemento-enamel junction to alveolar bone crest (CEJ–ABC) distance was measured at the distal aspect of each maxillary first molar in ImageJ; the two sides were averaged to yield one value per rat. The interproximal region between the distobuccal root of the first molar and the mesiobuccal root of the second molar, bounded coronally by the first slice showing the CEJ and apically by the last slice containing the distal root of the first molar, was analysed in CTAn for bone volume fraction (BV/TV), trabecular separation (Tb.Sp) and scanner-reported bone mineral density (BMD; g/cm^3). Bilateral micro-CT measurements were summarized within each rat before group comparison.

Histology and immunohistochemistry

Fixed maxillae were decalcified in 10% EDTA for 4 weeks, embedded in paraffin and sectioned at 3 μm. Sections were stained with haematoxylin and eosin, Masson's trichrome or tartrate-resistant acid phosphatase (TRAP), or processed for immunohistochemistry. Antigens were retrieved at 90 °C for 30 min in EDTA buffer at pH 8.0 for IL-6 and pH 9.0 for TNF-α. Rabbit primary antibodies against IL-6 (GB11117, 1:200) and TNF-α (GB115701, 1:500; both Servicebio) were detected with an S-vision goat anti-rabbit polymer secondary antibody (Online Resource Table S3). Sections were scanned with a Saiviewer LG-FS80. In the interradicular region, TRAP-positive multinucleated cells lining alveolar bone were counted per mm^2; IL-6- and TNF-α-positive cells were expressed as a percentage of all cells. Values from multiple sections were averaged to obtain one value per rat.

Statistical analysis

Data are presented as mean ± SEM (three independent donors for cellular experiments; four rats per group for animal experiments). Bilateral measurements and histological subsamples were averaged within each rat before analysis. Four-group comparisons, including all micro-CT and histological endpoints, were analysed by one-way ANOVA. Time-course data were analysed by two-way ANOVA. Pairwise comparisons used Tukey's multiple-comparisons test (GraphPad Prism 8.0). Tests were two-sided, with adjusted $P < 0.05$ considered significant for pairwise comparisons.

Results

Eu-HAP nanorods retain the apatite phase and rod morphology of HAP

The XRD patterns of both materials matched the hydroxyapatite reference (JCPDS 09-0432), with no additional resolved reflections (Fig. 2A). FTIR showed phosphate absorption near 1030 cm^{-1} together with C–H (2924 and 2853 cm^{-1}), carboxylate (1555 and 1456 cm^{-1}) and O–H (3421 cm^{-1}) bands in oleate-capped Eu-HAP before PEGylation (Fig. 2B). TEM showed rod-shaped particles in both preparations (Fig. 2C), and elemental mapping showed Ca, P, O and Eu distributed across Eu-HAP nanorods (Fig. 2D). ICP-OES measured 8.0 wt% Eu in Eu-HAP and no detectable Eu in HAP (Fig. 2E). Using the measured Ca content of 14.7 wt%, the bulk Eu/(Ca + Eu) molar fraction was 12.5%, calculated as (8.0/151.964)/[(8.0/151.964) + (14.7/40.078)]. This bulk elemental ratio exceeded the 5% feed fraction. Ca and P contents were 14.7 and 7.0 wt% in Eu-HAP and 27.0 and 11.5 wt% in HAP. PEGylated Eu-HAP in water had a zeta potential of −22.1 mV, a hydrodynamic diameter of 321 nm and a polydispersity index of 0.055 (Fig. 2F, G); the DLS diameter describes the dispersed particles rather than TEM rod length.

Cytocompatibility screening supports a 10 μg/mL working concentration

Live/dead staining after 48 h showed predominantly calcein-positive cells at 10–100 μg/mL for both materials, with propidium-iodide-positive cells apparent at 200 μg/mL (Fig. 3A, B). CCK-8 absorbance increased from day 1 to day 7 and did not fall below untreated values at concentrations up to 100 μg/mL (Fig. 3C, D). The 10 μg/mL concentration was selected because ALP activity peaked at this concentration in the osteogenic screening assays (Fig. 4A–D). The 50 μg/mL condition showed no apparent loss of cytocompatibility in these assays but provided no further increase in ALP activity or Alizarin Red S staining; 10 μg/mL was therefore carried forward.

Eu-HAP reduces inflammatory transcripts after LPS withdrawal

After LPS exposure and washout, DCF fluorescence was stronger in LPS-only cultures than in unchallenged cultures and appeared weaker after Eu-HAP treatment (Fig. 3E). At the transcript level, LPS increased *TNF* approximately 1.7-fold and *IL1B* 5.3-fold relative to the unchallenged group (Fig. 3F, G). Eu-HAP reduced both transcripts relative to HAP ($P < 0.05$ for *TNF*; $P < 0.0001$ for *IL1B*). *TNF* approached the unchallenged mean, whereas *IL1B* remained approximately 1.5 times that mean. Representative TNF-α and IL-1β immunofluorescence images showed qualitatively lower signals after Eu-HAP treatment (Fig. 3H, I). These images support the transcript observations but do not establish quantitative protein normalization.

Eu-HAP enhances selected osteogenic responses after LPS withdrawal

In LPS-challenged cultures, ALP staining and activity were highest at 10 μg/mL for both materials; values with 5–10 μg/mL Eu-HAP approached those in unchallenged cultures (Fig.

4A, C, D). Alizarin Red S staining on day 21 was most extensive with 10 μg/mL Eu-HAP (Fig. 4B). LPS reduced *ALPL*, *RUNX2* and *SPP1* transcripts on days 4 and 7 (Fig. 4E–G). HAP-treated cultures showed *ALPL* values of approximately 0.7- and 0.9-fold of control on days 4 and 7. With Eu-HAP, *ALPL* approached the control mean on day 4 and reached 2.2-fold on day 7 ($P < 0.0001$ versus LPS and HAP). *SPP1* approached the control mean on day 7 and exceeded the HAP group ($P < 0.0001$). *RUNX2* increased relative to LPS ($P < 0.05$ on day 7) but did not differ significantly between Eu-HAP and HAP. ALP, RUNX2 and OPN immunofluorescence images provide qualitative support (Fig. 4H–J). The quantitative findings support an advantage of Eu-HAP for selected osteogenic endpoints, particularly ALPL and SPP1, rather than all markers.

Local Eu-HAP injection attenuates alveolar bone loss in ligature-induced periodontitis

At day 28, exposed root surfaces were most extensive in the ligature + saline group (Fig. 5A, B). Mean CEJ–ABC distances in untreated, ligature + saline, ligature + HAP and ligature + Eu-HAP rats were 0.18, 0.69, 0.58 and 0.44 mm, respectively (Fig. 5C). The Eu-HAP mean was 0.14 mm lower than the HAP mean (Tukey-adjusted $P = 0.0406$) and 0.25 mm lower than the saline mean ($P = 0.0012$). HAP did not differ significantly from saline ($P = 0.1564$). In the same group order, BV/TV was 82%, 65%, 73% and 80%; Tb.Sp was 0.12, 0.21, 0.15 and 0.13 mm; and scanner-reported BMD was 0.45, 0.37, 0.42 and 0.43 g/cm³ (Fig. 5D–F). Compared with HAP, Eu-HAP had a 7-percentage-point higher BV/TV ($P = 0.0492$); the groups did not differ significantly in Tb.Sp ($P = 0.4408$) or BMD ($P = 0.4070$). All pairwise comparisons are reported in Online Resource Table S4. These endpoint measurements support preservation of residual alveolar bone. Without a pretreatment scan or dynamic bone labels, they do not establish new attachment, cementum formation or periodontal regeneration.

Eu-HAP preserves periodontal architecture and reduces osteoclast density

Haematoxylin and eosin and Masson's trichrome staining showed disrupted periodontal architecture and inflammatory infiltration after ligature + saline, partial preservation with HAP, and better-preserved crestal bone and collagen with Eu-HAP (Fig. 6A, B). TRAP-positive osteoclast density increased from virtually none in untreated rats to 59 cells/mm² with saline and was 39 cells/mm² with HAP and 21 cells/mm² with Eu-HAP ($P < 0.05$ versus HAP; Fig. 6C, D). IL-6-positive cells accounted for 4.2% in untreated rats, 5.7% with saline, 5.4% with HAP and 4.3% with Eu-HAP (Fig. 6E, F). TNF-α-positive cell fractions changed in the same direction, but differences were not statistically significant (Fig. 6G, H). Thus, the histological findings support lower osteoclast density and IL-6-positive cell fractions with Eu-HAP, without establishing a reduction in tissue TNF-α.

Discussion

Eu-HAP reduced inflammatory transcripts and enhanced selected osteogenic responses in primary hPDLCs after LPS withdrawal. In rats, local administration from day 7 reduced endpoint alveolar bone loss, with smaller CEJ–ABC distances and higher BV/TV than HAP. Osteoclast density was approximately two-thirds lower than with saline. The contribution of this study is the evaluation of a locally administered Eu-HAP formulation in periodontal disease, combining primary human ligament-cell responses after an inflammatory insult with bone preservation in a ligature model. These complementary findings do not establish that the hPDLC response mediates the animal effect.

Eu accounted for 12.5 mol% of Eu and Ca in the product, compared with 5 mol% in the precursor feed. The feed contained 0.098 mmol Eu (14.89 mg), but feed-to-product mass balance was not measured. The bulk composition therefore cannot distinguish preferential Eu

incorporation from differential loss of Eu and Ca during processing. XRD and elemental mapping support an apatite-like structure containing Eu; they do not establish Eu site occupancy or exclude minor or amorphous phases. Both syntheses included NaF, but the extent of fluoride incorporation was not measured [18]. The formulations also differed in Ca and P mass fractions. Their biological effects are compared at the same material concentration and cannot be attributed to Eu alone.

Previous studies suggest several mechanisms worth testing: NF-κB-related inflammatory signalling in periodontal ligament cells [5, 7], altered oxidative and osteoclast responses to europium-containing nanospheres [15], and ERK-related signalling with other europium-containing materials [11, 13]. None was tested directly in the present hPDLC experiments. The concurrent reduction in inflammatory transcripts and increase in *ALPL* and *SPP1* expression identifies associated responses; determining whether one drives the other requires targeted perturbation. Similarly, weaker DCF fluorescence does not demonstrate direct ROS scavenging, and unquantified immunofluorescence cannot establish changes in protein abundance.

At 10 μg/mL, bilateral delivery of 20 μL per side supplied 0.4 μg Eu-HAP and 32 ng Eu per dosing date. Seven dosing dates delivered 2.8 μg Eu-HAP, equivalent to 224 ng Eu per rat. The working concentration came from the cellular dose screen. The three-day interval followed our previous ligature study [16]; it was not based on measured particle residence time. The mass of the exposed tissue and the distribution of the injectate were not measured, so administered Eu cannot be converted to a tissue concentration or compared directly with the local exposure from implanted scaffolds [9, 10].

Lower osteoclast density and less endpoint bone loss are consistent with reduced resorption. Serial imaging and bone-formation labels would distinguish preservation from bone formation during treatment. The ligatures remained in place throughout dosing, whereas the cell experiments examined recovery after LPS washout. Whether the formulation offers an additional benefit after subgingival instrumentation remains to be tested.

The animal study included four young male rats per group, one dose and one endpoint. Three independent donors provided biological replication in vitro but limited the assessment of donor variation. Density-phantom calibration could not be verified for BMD; interpretation therefore centres on CEJ–ABC distance and BV/TV. Material-associated optical or staining effects may also contribute to CCK-8, DCF, Alizarin Red S and red-channel immunofluorescence signals.

Biodistribution and systemic safety

Eu-HAP was delivered as a PEGylated aqueous suspension, so persistence at the injection site will depend on particle–tissue interactions, uptake and clearance. Dissolution and ion exchange are plausible degradation processes, but their rates and Eu speciation were not measured. Released Eu may associate with phosphate or biological ligands; the proportions retained locally or entering the circulation remain unknown. In a separate calcium phosphate nanoparticle study, soft-tissue administration produced predominantly local retention during short-term imaging, whereas intravenous administration led to lung uptake and subsequent liver and spleen redistribution [23]. This route dependence supports measuring biodistribution directly for the periodontal formulation.

Systemic safety was not assessed. If particles or released Eu enter the circulation, the liver, spleen, kidneys and mineralized tissues are relevant sites for exposure assessment. Rare-earth oxide nanoparticles have caused phosphate-dependent lysosomal injury and inflammatory responses in experimental systems [24]; these observations identify hazards to investigate and do not establish toxicity of Eu-HAP. Administered Eu mass alone does not define a safety margin. Serial Eu measurements in blood, periodontal tissue, organs and excreta, together with

haematology, renal and liver biochemistry, histopathology and Eu-speciation analysis, are needed to characterize accumulation, elimination and adverse effects after repeated local dosing.

Conclusion

Eu-HAP lowered *TNF* and *IL1B* expression and enhanced *ALPL* and *SPP1* expression relative to HAP in primary periodontal ligament cells after LPS withdrawal. In ligature-treated rats, Eu-HAP was associated with a shorter endpoint CEJ–ABC distance, higher BV/TV and lower osteoclast density than HAP. These findings support further study of local Eu-HAP for periodontal bone preservation.

Declarations

Funding This work was supported by the National Natural Science Foundation of China (11932012 and 32171348), the National Key Research and Development Program of China (2022YFC2405904), the Innovative Research Team of High-level Local Universities in Shanghai (SHSMU-ZLCX20212402) and the Fundamental Research Program Funding of Ninth People's Hospital Affiliated to Shanghai Jiao Tong University School of Medicine (JYZZ085).

Competing interests The authors declare that they have no known competing financial interests or personal relationships that could have appeared to influence the work reported in this paper.

Ethics approval Animal procedures were approved by the Laboratory Animal Ethics Committee of Shanghai Ninth People's Hospital, Shanghai Jiao Tong University School of Medicine (SH9H-2023-A825-1). Collection and use of human periodontal ligament tissue from the study donors were approved by the Ethics Committee of Shanghai Ninth People's Hospital (SH9H-2024-T251-1), in accordance with the Declaration of Helsinki and applicable institutional requirements.

Participants were informed of the study procedures and their right to withdraw. Written informed consent was obtained from donors and, for minors, from a parent or legal guardian; assent was obtained where applicable. Samples and personal information were anonymized, and no identifiable participant data are reported.

Consent to participate Written informed consent was obtained from all tissue donors and, for donors under the age of majority, from a parent or legal guardian.

Consent for publication Not applicable; the manuscript contains no individually identifiable data.

Data availability The data supporting the findings of this study are available from the corresponding authors on reasonable request.

Author contributions Yangyang Jiang: conceptualization, formal analysis, project administration, writing – original draft. Junqin Lu: conceptualization, resources, writing – original draft. Tiancheng Li: methodology, data curation, visualization. Cheng Zhu: resources, project administration. Ruomei Li: investigation. Zhiyu Zhu: investigation. Jin Hao: resources, supervision, writing – review and editing. Lunguo Xia: conceptualization, funding acquisition, supervision, writing – review and editing. Bing Fang: funding acquisition, supervision, writing – review and editing.

Acknowledgements Schematic illustrations were created with BioRender.

References

1. Kinane DF, Stathopoulou PG, Papapanou PN (2017) Periodontal diseases. Nat Rev Dis Primers 3:17038. https://doi.org/10.1038/nrdp.2017.38

2. Chen MX, Zhong YJ, Dong QQ, Wong HM, Wen YF (2021) Global, regional, and national burden of severe periodontitis, 1990–2019: an analysis of the Global Burden of Disease Study 2019. J Clin Periodontol 48:1165–1188. https://doi.org/10.1111/jcpe.13506

3. Sanz M, Herrera D, Kebschull M, et al (2020) Treatment of stage I–III periodontitis—The EFP S3 level clinical practice guideline. J Clin Periodontol 47(Suppl 22):4–60. https://doi.org/10.1111/jcpe.13290

4. Luan J, Li R, Xu W, Sun H, Li Q, Wang D, Dong S, Ding J (2023) Functional biomaterials for comprehensive periodontitis therapy. Acta Pharm Sin B 13:2310–2333. https://doi.org/10.1016/j.apsb.2022.10.026

5. Kato H, Taguchi Y, Tominaga K, Umeda M, Tanaka A (2014) Porphyromonas gingivalis LPS inhibits osteoblastic differentiation and promotes pro-inflammatory cytokine production in human periodontal ligament stem cells. Arch Oral Biol 59:167–175. https://doi.org/10.1016/j.archoralbio.2013.11.008

6. Sun J, Wang Z, Liu P, Hu Y, Li T, Yang J, Gao P, Xu Q (2022) Exosomes derived from human gingival mesenchymal stem cells attenuate the inflammatory response in periodontal ligament stem cells. Front Chem 10:863364. https://doi.org/10.3389/fchem.2022.863364

7. Hu Y, Wang Z, Fan C, Gao P, Wang W, Xie Y, Xu Q (2023) Human gingival mesenchymal stem cell-derived exosomes cross-regulate the Wnt/β-catenin and NF-κB signalling pathways in the periodontal inflammation microenvironment. J Clin Periodontol 50:796–806. https://doi.org/10.1111/jcpe.13798

8. Zhou H, Lee J (2011) Nanoscale hydroxyapatite particles for bone tissue engineering. Acta Biomater 7:2769–2781. https://doi.org/10.1016/j.actbio.2011.03.019

9. Liu M, Zhou G, Hou Y, Kuang G, Jia Z, Li P, Fan Y (2021) Luminescent net-like inorganic scaffolds with europium-doped hydroxyapatite for enhanced bone reconstruction. Nanoscale 13:1181–1194. https://doi.org/10.1039/D0NR05608A

10. Feng S, Peng X, Wu Y, et al (2024) Europium-doped three-dimensional porous calcium phosphate scaffolds as a strategy for facilitating the comprehensive regeneration of bone tissue: in vitro and in vivo. ACS Biomater Sci Eng 10:7086–7099. https://doi.org/10.1021/acsbiomaterials.4c01067

11. Jin Y, Shu M, Liu Z, Li H, Liu C, Zhu C, Zhu Z, Fang B, Xia L (2024) Bio-functional immunomodulatory europium-doped hydroxyapatite nanorods for osteochondral repair via CDH5-RAS-RAF-MEK-ERK-CSF1 axis. Chem Eng J 484:149311. https://doi.org/10.1016/j.cej.2024.149311

12. Martinez FM, Juárez-Moreno K, Vázquez L, Herrera M, Graeve OA (2026) Osteogenic potential and hemocompatibility of rare-earth-doped hydroxyapatite in murine preosteoblast cells. ACS Biomater Sci Eng 12:866–877. https://doi.org/10.1021/acsbiomaterials.5c01417

13. Shi M, Xia L, Chen Z, Lv F, Zhu H, Wei F, Han S, Chang J, Xiao Y, Wu C (2017) Europium-doped mesoporous silica nanosphere as an immune-modulating osteogenesis/angiogenesis agent. Biomaterials 144:176–187.

https://doi.org/10.1016/j.biomaterials.2017.08.027

14. Fernández-Villa D, Aguilar MR, Rojo L (2024) Europium–tannic acid nanocomplexes devised for bone regeneration under oxidative or inflammatory environments. J Mater Chem B 12:7153–7170. https://doi.org/10.1039/D4TB00697F

15. Wang YC, Cai MT, Chen MH, Tung FI, Chen MH, Liu TY (2024) Europium-containing nanospheres for treating ovariectomy-induced osteoporosis: targeted bone remodeling and macrophage polarization modulation. Int J Nanomedicine 19:10145–10163. https://doi.org/10.2147/IJN.S472253

16. Zhu Z, Li R, Mei P, Zhu C, Li T, Li Y, Tan W, Yang Y, Jin Y, Guo W, Fang R, Xia L, Fang B (2025) Lithium-doped silicon-hydroxyapatite nanowires alleviate early bone loss in periodontitis via γδ T cell modulation. Chem Eng J 519:165072. https://doi.org/10.1016/j.cej.2025.165072

17. Percie du Sert N, Hurst V, Ahluwalia A, et al (2020) The ARRIVE guidelines 2.0: updated guidelines for reporting animal research. PLoS Biol 18:e3000410. https://doi.org/10.1371/journal.pbio.3000410

18. Hui J, Wang X (2011) Luminescent, colloidal, F-substituted, hydroxyapatite nanocrystals. Chem Eur J 17:6926–6930. https://doi.org/10.1002/chem.201100680

19. Liu B, Deng X, Xie Z, Cheng Z, Yang P, Lin J (2017) Thiol–ene click reaction as a facile and general approach for surface functionalization of colloidal nanocrystals. Adv Mater 29:1604878. https://doi.org/10.1002/adma.201604878

20. Gregory CA, Gunn WG, Peister A, Prockop DJ (2004) An Alizarin red-based assay of mineralization by adherent cells in culture: comparison with cetylpyridinium chloride extraction. Anal Biochem 329:77–84. https://doi.org/10.1016/j.ab.2004.02.002

21. Abe T, Hajishengallis G (2013) Optimization of the ligature-induced periodontitis model in mice. J Immunol Methods 394:49–54. https://doi.org/10.1016/j.jim.2013.05.002

22. Chipashvili O, Utter DR, Bedree JK, et al (2021) Episymbiotic Saccharibacteria suppresses gingival inflammation and bone loss in mice through host bacterial modulation. Cell Host Microbe 29:1649–1662.e7. https://doi.org/10.1016/j.chom.2021.09.009

23. Kollenda SA, Klose J, Knuschke T, Sokolova V, Schmitz J, Staniszewska M, Fragoso Costa P, Herrmann K, Westendorf AM, Fendler WP, Epple M (2020) In vivo biodistribution of calcium phosphate nanoparticles after intravascular, intramuscular, intratumoral, and soft tissue administration in mice investigated by small animal PET/CT. Acta Biomater 109:244–253. https://doi.org/10.1016/j.actbio.2020.03.031

24. Li R, Ji Z, Chang CH, et al (2014) Surface interactions with compartmentalized cellular phosphates explain rare earth oxide nanoparticle hazard and provide opportunities for safer design. ACS Nano 8:1771–1783. https://doi.org/10.1021/nn406166n

Figure legends

Fig. 1 Schematic overview of hydrothermal Eu-HAP synthesis, PEGylation, treatment of hPDLCs following a 24-h LPS challenge and washout, and local administration in ligature-induced periodontitis. The cell and animal experiments are complementary components of the study; the diagram does not establish mediation of the animal response by hPDLCs.

Fig. 2 Physicochemical characterization of HAP and Eu-HAP nanorods. (A) XRD patterns of HAP and Eu-HAP with the hydroxyapatite reference pattern (JCPDS 09-0432). (B) FTIR spectrum of oleate-capped Eu-HAP. (C) TEM images of HAP (upper row) and Eu-HAP (lower

row) at increasing magnification; scale bars 200, 100, 50, 20 and 10 nm from left to right. (D) Dark-field STEM image and elemental maps of Ca, Eu, O and P in Eu-HAP; scale bars 100 nm. (E) Ca, P and Eu content of both materials by ICP-OES (mean ± SEM, n = 3). (F) Zeta-potential distribution and (G) volume-weighted hydrodynamic size distribution of PEGylated Eu-HAP in deionized water (0.1% w/v, pH 7, 25 °C).

Fig. 3 Cytocompatibility and inflammatory responses after LPS withdrawal. (A, B) Calcein-AM (green) and propidium iodide (red) staining after 48 h with HAP (A) or Eu-HAP (B); columns show 0 (control), 10, 50, 100 and 200 μg/mL. Scale bars, 200 μm. (C, D) CCK-8 absorbance on days 1, 4 and 7 with HAP (C) or Eu-HAP (D) at 0, 5, 10, 50, 100 or 200 μg/mL. (E–I) Blank, unchallenged cells; LPS, material-free medium after a 24-h LPS challenge; LPS + HAP and LPS + Eu-HAP, 10 μg/mL of the indicated material after LPS washout. LPS was not replenished. (E) DCF fluorescence (green) and Hoechst counterstain (blue), acquired at identical camera settings across groups; scale bar, 250 μm. (F, G) *TNF* (F) and *IL1B* (G) mRNA after 4 days of treatment. (H, I) Representative TNF-α (H) and IL-1β (I) immunofluorescence (red), F-actin (green) and nuclei (blue); scale bars, 200 μm. Fluorescence images were acquired at identical settings across groups and assessed qualitatively. Quantitative data are mean ± SEM, n = 3 independent donors. *P < 0.05, **P < 0.01, ***P < 0.001, ****P < 0.0001; ns, not significant.

Fig. 4 Osteogenic responses after LPS withdrawal. (A) ALP staining on day 4 and (B) Alizarin Red S staining on day 21 with 0, 5, 10 or 50 μg/mL HAP or Eu-HAP. (C, D) ALP activity normalized to total protein. (E–G) *ALPL*, *RUNX2* and *SPP1* mRNA on days 4 and 7. (H–J) Representative ALP, RUNX2 and OPN immunofluorescence (red), F-actin (green) and nuclei (blue); scale bars 200 μm. LPS was washed out after 24 h and was not replenished. Blank denotes no LPS; 0 μg/mL and LPS denote challenged cultures without material. HAP10 and Eu-HAP10 denote 10 μg/mL material after LPS withdrawal. The 50 μg/mL condition showed no apparent loss of cytocompatibility (Fig. 3) and no additional increase in ALP activity or Alizarin Red S staining above 10 μg/mL; the latter was selected as the working concentration. Alizarin Red S and immunofluorescence images are qualitative; immunofluorescence intensity was not quantified. Quantitative data are mean ± SEM, n = 3 independent donors. *P < 0.05, **P < 0.01, ***P < 0.001, ****P < 0.0001.

Fig. 5 Endpoint alveolar bone measurements in the rat ligature model. (A) Timeline. Ligatures remained in place; bilateral injections were given on days 7, 10, 13, 16, 19, 22 and 25, and maxillae were collected on day 28. (B) Representative buccal micro-CT reconstructions; exposed root surfaces are shaded red. (C) CEJ–ABC distance at the distal aspect of the maxillary first molar. (D–F) BV/TV, Tb.Sp and scanner-reported BMD in the interproximal region. Bars show mean ± SEM, n = 4 rats/group, after averaging bilateral measurements within each rat. For Eu-HAP versus HAP, Tukey-adjusted P values were 0.0406 for CEJ–ABC, 0.0492 for BV/TV, 0.4408 for Tb.Sp and 0.4070 for BMD (one-way ANOVA). Symbols denote comparisons with untreated (*), ligature + saline (#) or ligature + HAP (&); *P < 0.05, **P < 0.01, ***P < 0.001; the same thresholds apply to # and &. All pairwise P values are given in Online Resource Table S4.

Fig. 6 Periodontal histology at day 28. (A) Haematoxylin and eosin and (B) Masson's trichrome staining. PDL, periodontal ligament; AB, alveolar bone; D, dentin; C, cementum. (C) TRAP staining (arrows, TRAP-positive osteoclasts) and (D) osteoclast density. (E, F) IL-6 immunostaining and positive-cell fraction; (G, H) TNF-α immunostaining and positive-cell fraction. The rabbit primary antibodies were diluted 1:200 for IL-6 and 1:500 for TNF-α; heat retrieval was performed at 90 °C for 30 min in EDTA at pH 8.0 and 9.0, respectively (Online Resource Table S3). Boxed regions are enlarged below each overview. Scale bars: 200 μm in overviews and 100 μm in enlargements (A, B, C, E, G). Values from multiple sections were

averaged within each rat. Mean ± SEM, n = 4 rats/group; one-way ANOVA with Tukey's post hoc test. *P < 0.05, **P < 0.01, ***P < 0.001, ****P < 0.0001. Between-group differences in TNF-α staining were not statistically significant.

Fig. 1

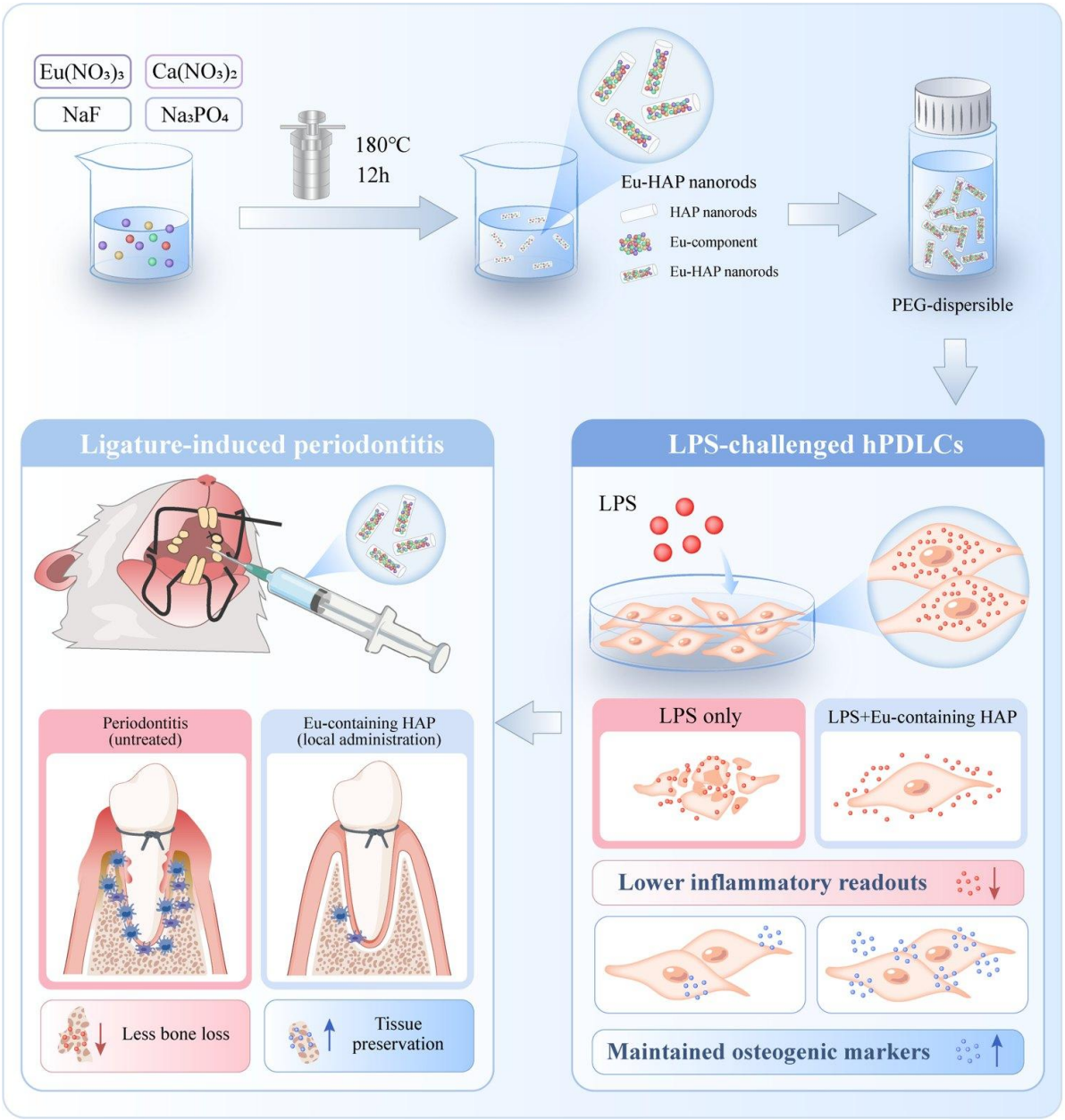

Eu(NO3)3
Ca(NO3)2
NaF
Na3PO4
180°C
12h
Eu-HAP nanorods
HAP nanorods
Eu-component
Eu-HAP nanorods
PEG-dispersible
Ligature-induced periodontitis
Periodontitis (untreated)
Eu-containing HAP (local administration)
Less bone loss
Tissue preservation
LPS-challenged hPDLCs
LPS
LPS only
LPS+Eu-containing HAP
Lower inflammatory readouts
Maintained osteogenic markers

Fig. 2

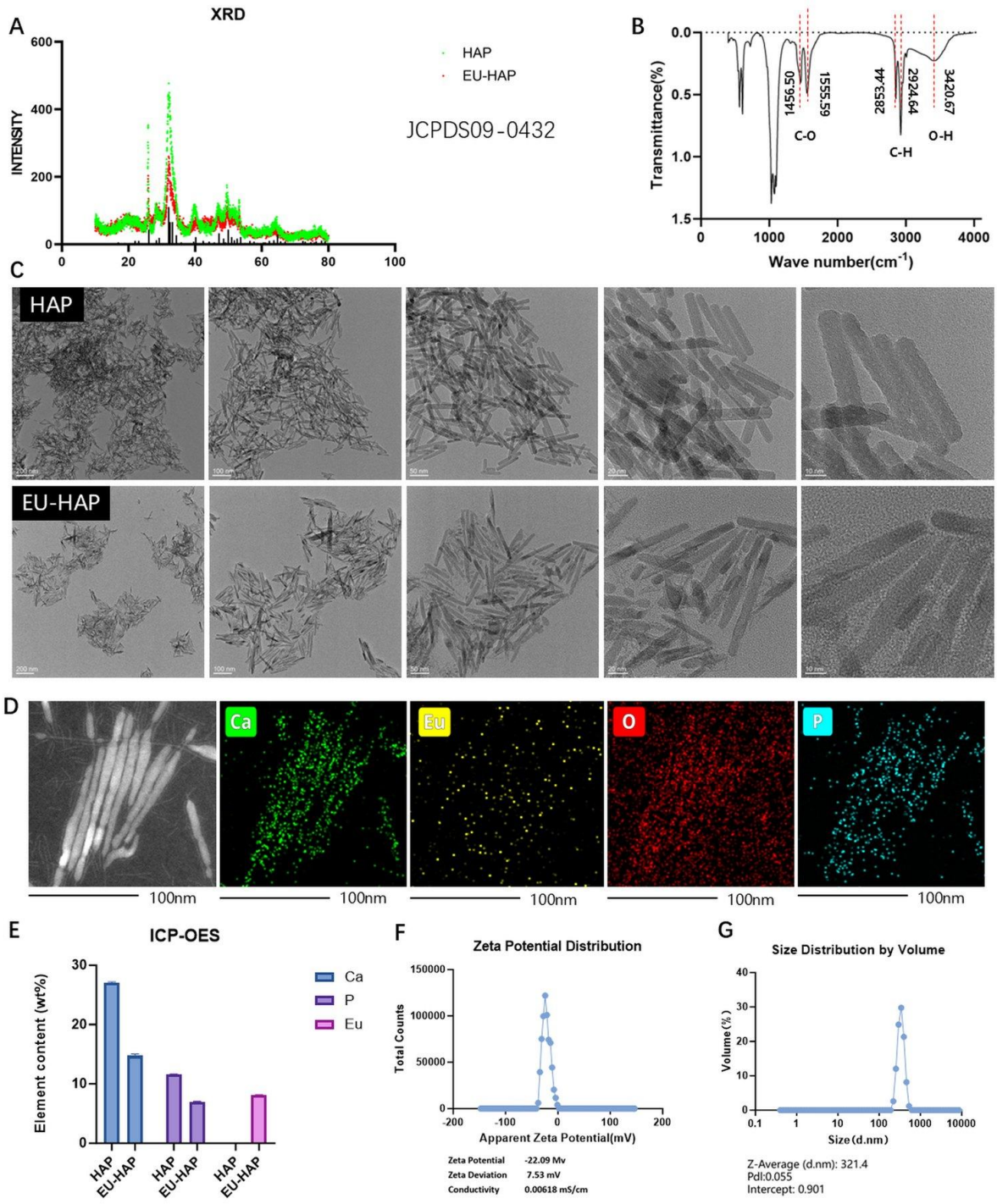
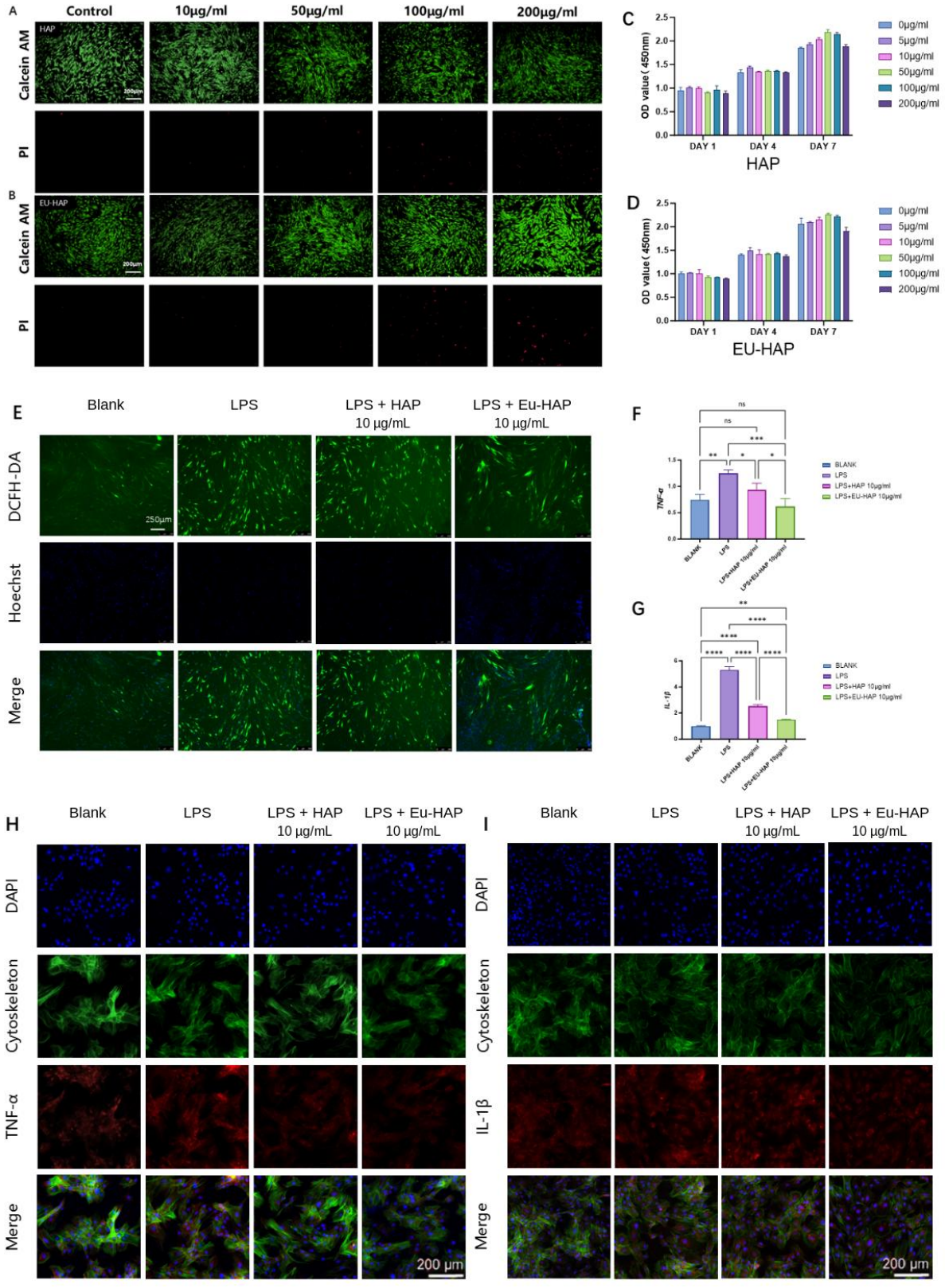
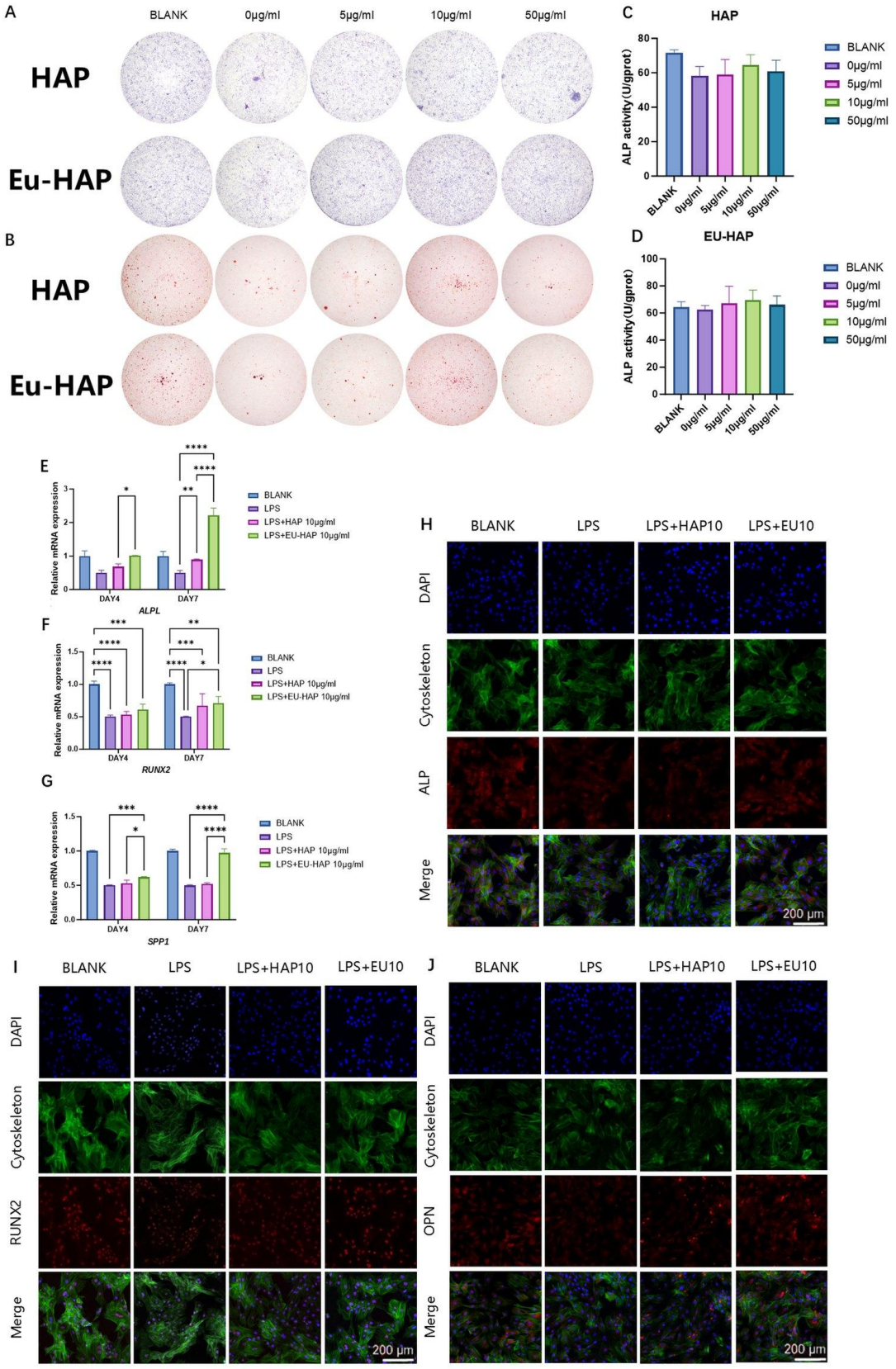

A
XRD
HAP
EU-HAP
JCPDS09-0432
INTENSITY
B
Transmittance(%)
1456.50
1555.59
2853.44
2924.64
3420.67
C-O
C-H
O-H
Wave number(cm-1)
C
HAP
EU-HAP
D
Ca
Eu
O
P
100nm
E
ICP-OES
Element content (wt%)
Ca
P
Eu
HAP
EU-HAP
F
Zeta Potential Distribution
Total Counts
Apparent Zeta Potential(mV)
Zeta Potential -22.09 Mv
Zeta Deviation 7.53 mV
Conductivity 0.00618 mS/cm
G
Size Distribution by Volume
Volume(%)
Size(d.nm)
Z-Average (d.nm): 321.4
PdI:0.055
Intercept: 0.901

Fig. 3


A
Control
10μg/ml
50μg/ml
100μg/ml
200μg/ml
Calcein AM
HAP
PI
B
EU-HAP
C
OD value (450nm)
DAY 1
DAY 4
DAY 7
HAP
0μg/ml
5μg/ml
10μg/ml
50μg/ml
100μg/ml
200μg/ml
D
EU-HAP
E
Blank
LPS
LPS + HAP 10 μg/mL
LPS + Eu-HAP 10 μg/mL
DCFH-DA
Hoechst
Merge
250μm
F
TNF-α
G
IL-1β
BLANK
LPS
LPS+HAP 10μg/ml
LPS+EU-HAP 10μg/ml
H
DAPI
Cytoskeleton
TNF-α
200 μm
I
IL-1β

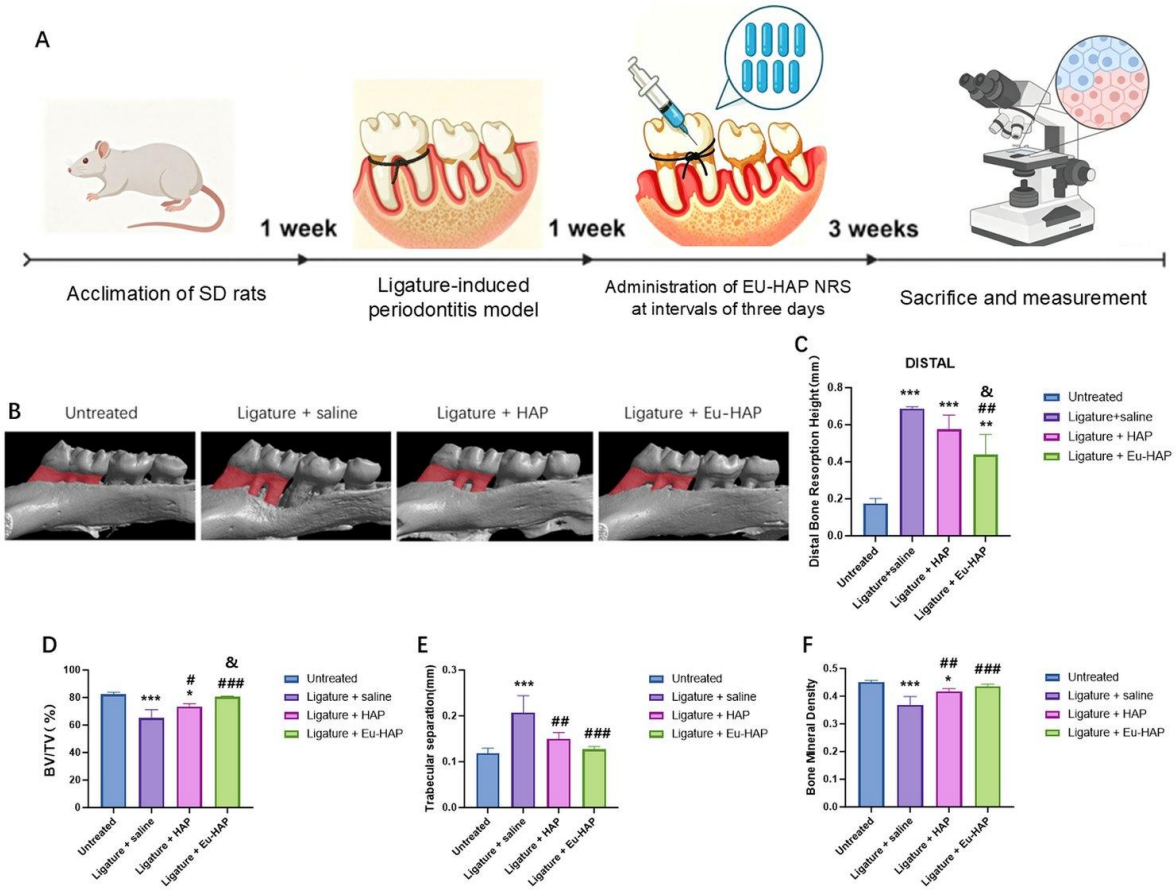
633 **Fig. 4**



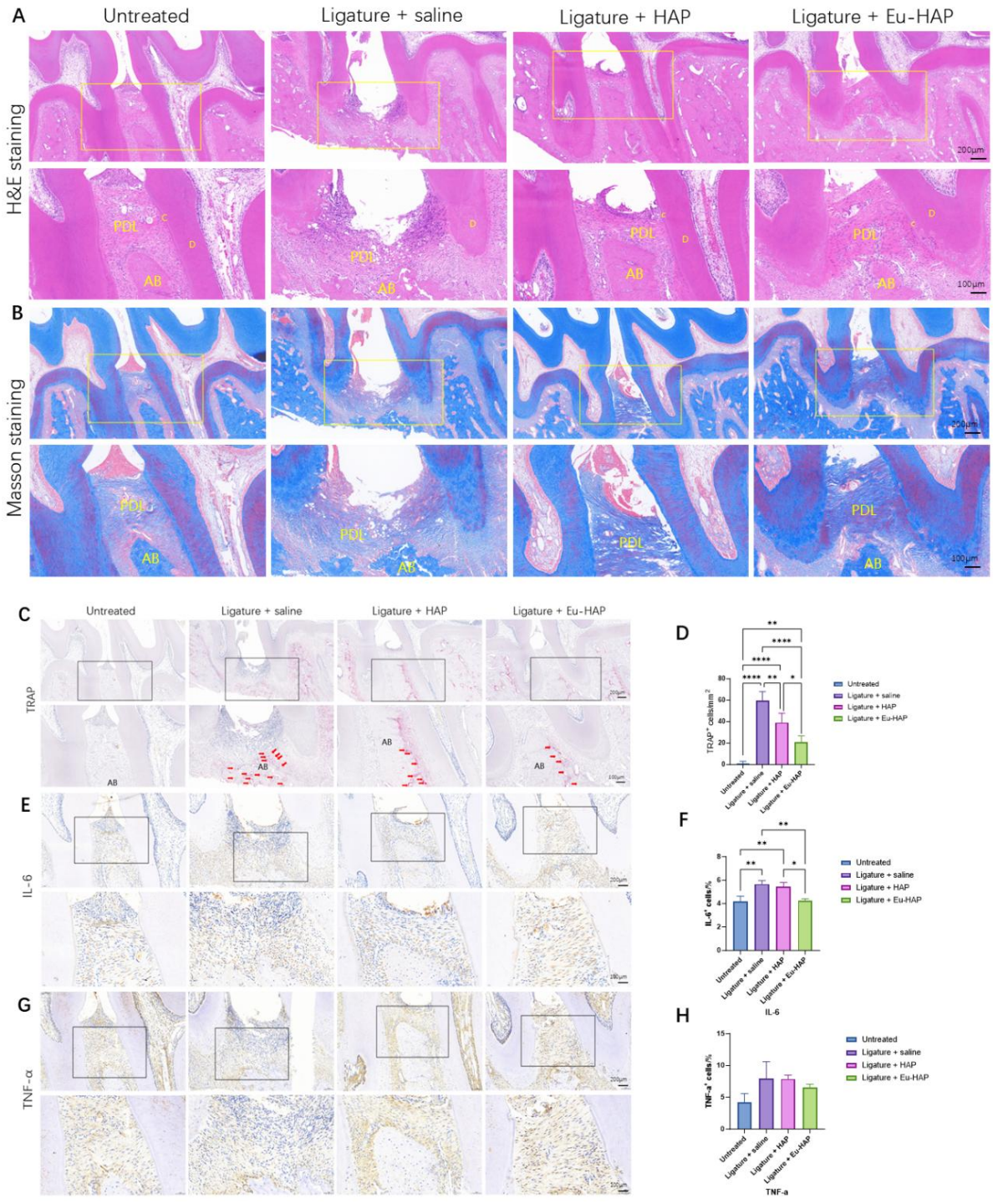
634
635

636

Fig. 5


A
1 week
1 week
3 weeks
Acclimation of SD rats
Ligature-induced periodontitis model
Administration of EU-HAP NRS at intervals of three days
Sacrifice and measurement
B
Untreated
Ligature + saline
Ligature + HAP
Ligature + Eu-HAP
C
DISTAL
Distal Bone Resorption Height(mm)
Untreated
Ligature+saline
Ligature + HAP
Ligature + Eu-HAP
D
BV/TV (%)
E
Trabecular separation(mm)
F
Bone Mineral Density

654 **Fig. 6**


A
Untreated
Ligature + saline
Ligature + HAP
Ligature + Eu-HAP
H&E staining
PDL
AB
B
Masson staining
C
TRAP
D
E
IL-6
F
G
TNF-α
H
Untreated
Ligature + saline
Ligature + HAP
Ligature + Eu-HAP
TRAP+ cells/mm2
IL-6+ cells/%
TNF-α+ cells/%
IL-6
TNF-a

655

Supplementary Files

This is a list of supplementary files associated with this preprint. Click to download.

- OnlineResourcetables.docx